

A Waveguide Verification Standard Design Procedure for the Microwave Characterization of Magnetic Materials

Benjamin R. Crowgey, Junyan Tang, Edward J. Rothwell*,
Balasubramaniam Shanker, and Leo C. Kempel

Abstract—A waveguide standard is introduced for validation purposes on the measurement accuracy of electric and magnetic properties of materials at microwave frequencies. The standard acts as a surrogate material with both electric and magnetic properties and is useful for verifying systems designed to characterize engineered materials using the Nicolson-Ross-Weir technique. A genetic algorithm is used to optimize the all-metallic structure to produce a surrogate with both relative permittivity and permeability within a target range across S-band. A mode-matching approach allows the user to predict the material properties with high accuracy, and thus compensate for differences in geometry due to loose fabrication tolerances or limited availability of component parts. The mode-matching method also allows the user to design standards that may be used within other measurement bands. An example standard is characterized experimentally, the errors due to uncertainties in measured dimensions and to experimental repeatability are explored, and the usefulness of the standard as a verification tool is validated.

1. INTRODUCTION

The use of engineered materials in the design of radio frequency (RF) systems requires an accurate knowledge of material constitutive parameters. Some recently synthesized materials include graphene nanoribbons or metallic inclusions for use in miniaturization of electronic components [1, 2], ferrite loaded polymers to increase EMI shielding [3], cellular materials such as honeycomb structures to decrease radar cross-section [4], and anisotropic materials used to enhance antenna operation [5]. Since the properties of these materials are often hard to accurately predict (due to modeling uncertainties and variability in the manufacturing process), they are usually measured in a laboratory.

Rectangular waveguide applicators are commonly used to extract the electromagnetic properties of materials. Benefits over alternative methods, such as free-space systems, include the availability of analytical expressions to describe sample interrogation, high signal strength, and the simplicity of manufacturing rectangular samples [6–9]. The S -parameters measured with a material sample placed in the cross-sectional plane of a waveguide may be used to determine the complex values of the permittivity, $\epsilon = \epsilon_0(\epsilon'_r - j\epsilon''_r)$, and the permeability, $\mu = \mu_0(\mu'_r - j\mu''_r)$, from closed-form expressions [13, 14].

The accuracy of a material characterization system is often established by measuring a standard material with known properties. A desirable standard material is easy to machine, is stable thermally and chemically, is readily available, and has values of constitutive parameters numerically close to those of samples of interest with only minor variations within the measurement band. If the permittivity of materials is of primary interest, a dielectric sample such as Rexolite[®] may be used to provide highly-predictable parameters in the microwave spectrum with a value characteristic of many plastics [15].

Received 5 October 2014, Accepted 18 November 2014, Scheduled 19 December 2014

* Corresponding author: Edward J. Rothwell (rothwell@egr.msu.edu).

The authors are with the Department of Electrical and Computer Engineering, Michigan State University, East Lansing, MI 48824, USA.

The recent introduction of engineered materials with magnetic as well as dielectric properties has made it more difficult to find standard test materials whose constitutive parameters are known with great accuracy and have appropriate values within the microwave spectrum. Fortunately, it is possible to create a surrogate material sample that can act as the standard test material in the sense that its use in a material measurement system will produce extracted constitutive parameters with predictable, highly-accurate, and appropriate values. The surrogate need not resemble an actual material, and in fact can be inhomogeneous and non-magnetic. The only requirement is that when inserted in place of a test material, the surrogate provides proper S -parameters that may be used in the extraction process. Although some previous work has been done to create waveguide standards using circuits, obstacles, or components [16], these fabricated structures are only meant to validate the reflection and transmission coefficients, not the extracted material parameters.

It is crucial that a material standard produce highly accurate, stable, and repeatable values of extracted permittivity and permeability across the measurement band. It must be reproducible for the majority of users, and thus should be of simple design and made from readily available materials. The values of the extracted constitutive parameters should not be overly sensitive to the geometrical dimensions of the standard, so that errors in fabrication or changes in the operating environment (temperature, humidity, etc.) do not cause unpredictable or unacceptable results. Additionally, the values of permittivity and permeability must be predictable to high accuracy using standard, reproducible analytic techniques. For these reasons, the design adopted for the surrogate described here uses two simple metallic waveguide windows, or apertures, separated by a spacer. Given just four geometrical parameters, mode-matching techniques can be used to accurately compute the S -parameters of the surrogate material, and from these the extracted constitutive parameters may be determined. A description of the design process used to obtain an optimized geometry and a typical design for S-band using standard WR-284 dimensions are given below. The measured results for an example verification standard constructed from materials on hand are shown and discussed.

2. MATERIAL CHARACTERIZATION PROCEDURE

After a measurement setup has been calibrated appropriately [10–12], a verification standard provides confidence in the measuring system by producing known results under appropriate operating conditions, allowing the estimation of measurement accuracy. In the case of material characterization, the verification standard is placed into the system and known values of μ and ϵ are extracted using a specific algorithm. The standard described in this paper assumes the use of the classic “Nicolson-Ross-Weir” (NRW) extraction algorithm that employs the measured reflection and transmission coefficients for a waveguide section completely filled by the material [13, 14]. Other algorithms are available that use, for instance, only reflection measurements [17]; these would require a different standard. The attraction of the NRW characterization method results from the availability of closed-form expressions for μ and ϵ . This contrasts with methods requiring an iterative solver such as Newton’s method [18] or a least squares approach [19]. The convenience of the NRW method, and its insensitivity to propagation of measurement uncertainties, commonly makes it a first choice for material characterization. Since NRW extraction can be used with rectangular waveguides, coaxial applicators, free-space methods, and stripline measurements, the concept of the waveguide surrogate described here has wide applicability, although the details of the structural design vary from system to system.

Figure 1 shows the experimental configuration used in the NRW method. A sample with unknown properties is placed into a sample holder occupying the region $0 \leq z \leq d$ in a rectangular waveguide system. Waveguide extensions are usually employed to guarantee only the dominant mode is present at the measurement ports. The S -parameters S_{11} and S_{21} are measured using a vector network analyzer (VNA) attached at these ports, and the S -parameters are then mathematically transformed to obtain the S -parameters at the sample planes. These sample-plane S -parameters are used to determine the sample propagation constant β and the interfacial reflection coefficient Γ , which may in turn be used to find ϵ and μ as follows. Define $V_1 = S_{21} + S_{11}$ and $V_2 = S_{21} - S_{11}$. The interfacial reflection coefficient can be computed as

$$\Gamma = \frac{1 - V_1 V_2}{V_1 - V_2} \pm \sqrt{\left(\frac{1 - V_1 V_2}{V_1 - V_2}\right)^2 - 1}, \quad (1)$$

where the appropriate sign is chosen such that $|\Gamma| \leq 1$. Then the 1-way propagation factor for a wave traveling through the sample region can be written in terms of the computed Γ as

$$P = e^{-\gamma d} = \frac{V_1 - \Gamma}{1 - \Gamma V_1}, \quad (2)$$

such that $\gamma = (\ln P - j2n\pi)/(-d)$. Here n is an integer; its appropriate value depends on the length of the sample and is determined by requiring the resulting material parameters to obey physical constraints, such as passivity and continuity with frequency. Finally, the permittivity and permeability may be computed in closed form as

$$\mu = \mu_0 \frac{1 + \Gamma}{1 - \Gamma} \frac{\gamma}{j\beta_0}, \quad \epsilon = \epsilon_0 \left(\frac{\gamma\beta_0}{jk_0^2} \frac{1 - \Gamma}{1 + \Gamma} + \frac{\mu_0 k_c^2}{\mu k_0^2} \right), \quad (3)$$

where $k_0 = \omega\sqrt{\mu_0\epsilon_0}$, $\beta_0 = \sqrt{k_0^2 - k_c^2}$, and $k_c = \pi/a$. Note that the time convention $\exp(j\omega t)$ is used.

When the NRW method is used to extract μ and ϵ using arbitrary values of S_{11} and S_{21} , the resulting material parameters may not have the physical properties expected of actual materials. Thus, some care should be taken in designing the surrogate so that the measured S -parameters produce physically meaningful values of μ and ϵ . Since the proposed surrogate is constructed of nonmagnetic good conductors, it is worthwhile to examine the properties of μ and ϵ under lossless conditions (assuming the conductor losses in the surrogate may be ignored). It is shown in the appendix that it is useful to examine the quantity $A = \text{Re}\{S_{11}\}/|S_{11}|^2$. If $A^2 \geq 1$, then both ϵ and μ extracted using NRW are real, and thus represent a lossless material [20]. If $A^2 < 1$ then P is real, and if $P > 0$ and $n = 0$, both ϵ and μ are again real. However, if $A^2 < 1$ and $P < 0$, ϵ and μ are complex, and it is possible that either $\text{Im}\{\epsilon_r\} > 0$ or $\text{Im}\{\mu_r\} > 0$, or both. Since this condition implies gain, which is not possible with a passive surrogate, it is important to avoid this case when constructing a surrogate.

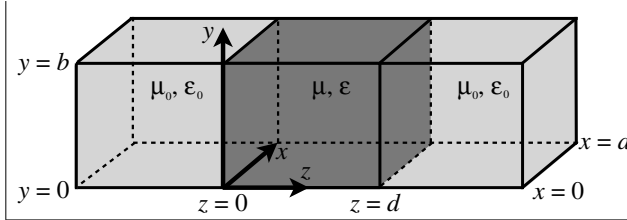


Figure 1. Waveguide material measurement system showing presence of material sample.

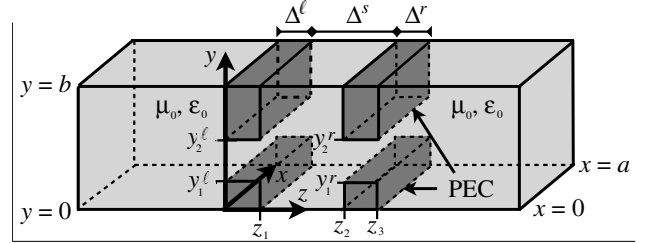


Figure 2. Waveguide material measurement system showing presence of the waveguide verification standard. Adopted surrogate has $\Delta^\ell = \Delta^r$, $y_1^\ell = y_1^r$, and $y_2^\ell = y_2^r$.

3. WAVEGUIDE VERIFICATION STANDARD DESIGN

It is important to develop a waveguide standard that is easily fabricated using materials readily available to most users. For this reason the surrogate was chosen to be constructed from purely nonmagnetic metallic parts, and in the following analysis is assumed to be perfectly conducting. After examining many candidate geometries, a simple structure consisting of two identical rectangular apertures of thickness $\Delta^\ell = \Delta^r$ separated by a spacer of thickness Δ^s as shown in Fig. 2 was adopted. The simple geometry of the adopted waveguide standard has several important advantages over more complex structures. First, it may be easily machined from simple metal sheets. Second, an easily implemented mode-matching technique may be used to analyze the structure quickly and with great accuracy, and thus commercial solvers are not required to determine the material properties of the surrogate. By controlling the accuracy of the analysis, the errors propagated to the extracted material parameters from uncertainties in the dimensions of the fabricated parts and from the uncertainties of the measured

S -parameters may be appropriately calculated. Third, if the standard is manufactured using materials of thicknesses different than those described in the optimized design, or if the manufactured apertures are somewhat offset from those of the optimized design, mode matching may be used to determine the theoretical properties of the manufactured standard, and the standard may still be used to verify the accuracy of a material measurement system.

The waveguide standard is placed into the measurement system in the same physical position as an unknown material; see Fig. 2. The length of the surrogate sample is $z_3 = d$ and thus the S -parameter planes are taken at $z = 0$ and $z = d$ as in the case of an actual sample. The NRW method assumes that the material sample is isotropic and homogeneous, and thus the measured S -parameters obey $S_{11} = S_{22}$ and $S_{12} = S_{21}$. Although it is not necessary that the waveguide standard be homogeneous, it is helpful if the S -parameters of the surrogate obey the same relationships as do those of an actual material. Thus, the waveguide standard should be symmetric in the longitudinal (z) direction. This allows the standard to be interrogated from either direction with identical results, and if the standard is constructed from lossless (or perfectly conducting) materials, it also allows the permittivity and permeability of the surrogate extracted using the NRW method to be purely real (corresponding to a lossless material), as discussed in the appendix. Unfortunately, if the surrogate is inhomogeneous along z , the real parts of the extracted permittivity and permeability will be frequency dependent, and thus the extracted parameters do not obey the Kronig-Kramers relations [22]. However, an inhomogeneous surrogate is still valuable as a verification standard since its material parameters can be tailored to a desired range and, if lossless, provide a quick check of the credibility of the measurements.

Materials with large but equal values of permittivity and permeability are desired for the construction of microwave antennas with enhanced radiation properties. Researchers are currently examining ways to synthesize such materials with the goal to achieve low-loss materials with relative permittivity and permeability in the 3–10 range at microwave frequencies [23]. Thus, the adopted design was tuned using a genetic algorithm (GA) with the goal to produce a surrogate material with both a permittivity and a permeability as near to six as possible across S-band, as found using NRW. The extracted parameters were also required to vary smoothly with frequency. The GA varied the vertical window positions (positions $y_1^\ell = y_1^r$ and $y_2^\ell = y_2^r$ in Fig. 1), horizontal window positions, and the thicknesses of the apertures and waveguide spacer, and used the commercial solver HFSS to compute S_{11} and S_{21} . The optimizer was configured for a combined 2-point and 3-point crossover with an evolving single bit mutation. Half of the new population was created by performing a two point crossover and the other half by performing a three point crossover. In both cases, the crossover points were selected randomly. An initial population of 100 different binary strings was selected randomly and the geometry of the waveguide standard was created in Matlab and exported to HFSS for simulation. See [24] for a detailed description of the GA algorithm.

The waveguide used is standard S-band WR-284 with dimensions $a = 2.84$ inch by $b = 1.34$ inch (72.136×34.036 mm) and a designated operational band of 2.6 to 3.95 GHz. The thicknesses of each aperture and spacer used during the GA optimization were limited to the values of United States standard brass stock (multiples of 1/16 inch, or 1.5875 mm), to simplify the fabrication process. To produce a symmetric verification standard, the apertures were assigned identical openings. The

Table 1. Dimensions of the optimized waveguide standard, and measured dimensions of the fabricated standard.

Dimension	Optimized Value (mm)	Fabricated Value (mm)	Difference (%)
Δ^ℓ	3.175	3.62 ± 0.03	14.0
Δ^r	3.175	3.57 ± 0.04	12.4
Δ^s	12.700	12.35 ± 0.07	-2.8
y_1^ℓ	5.064	5.18 ± 0.06	2.3
y_2^ℓ	23.860	23.91 ± 0.11	0.2
y_1^r	5.064	5.28 ± 0.07	4.3
y_2^r	23.860	23.49 ± 0.11	-1.6

dimensions of the standard found by the GA are given in Table 1. The material parameters extracted using the NRW method from the HFSS simulated S -parameters of the optimized design are shown in Fig. 3. As expected, the imaginary part of the extracted parameters are zero (to computational accuracy) and the real parts are dependent on frequency. Note that the optimizer has produced a trade off between frequency variation, and values near to six.

Precise values for the material parameters produced by the optimized waveguide standard may be found by applying the mode-matching technique (see the following section for details.) To produce the mode-matching results, the number of terms, N , was chosen to guarantee an accuracy of 5 digits in each of the extracted material parameters. This gives accuracy commensurate to what can be measured with the Agilent E5071C VNA used in subsequent experiments. In all cases, convergence was obtained with at most $N = 275$ modes. The resulting extracted material values are listed in Table 2 and are plotted in Fig. 3. Only the real parts of ϵ_r and μ_r are shown in Table 2, since the imaginary parts are less than 10^{-5} . These tabulated values can be used to verify the operational accuracy of waveguide material parameters measurement systems in S-band. Similar standards may be devised for other waveguide bands using the mode-matching method.

Table 2. Real parts of relative material parameters for the optimized waveguide verification standard with dimensions shown in Table 1.

Frequency (GHz)	ϵ_r	μ_r
2.60	6.0356	7.8526
2.80	6.2509	6.8508
3.00	6.2403	6.2399
3.20	6.0908	5.8523
3.40	5.8457	5.6194
3.60	5.5254	5.5157
3.80	5.1342	5.5449
3.95	4.7889	5.6754

It is clear from Fig. 3 that the material parameters extracted from the S -parameters computed using mode matching are quite close to those extracted using HFSS simulations. However, it is important to note that computing S -parameters with the same accuracy using HFSS takes approximately 60 times longer than for mode matching on a 3.5 GHz Intel quad core processor with 24 GB of RAM. Thus, the faster mode-matching approach makes it possible to carry out computationally-intensive Monte Carlo error analysis used to evaluate the sensitivity of the fabricated standard to geometry uncertainties.

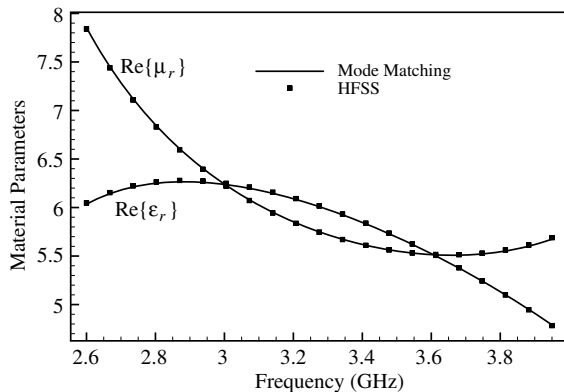


Figure 3. Material parameters extracted from S -parameter simulations of the optimized verification standard.

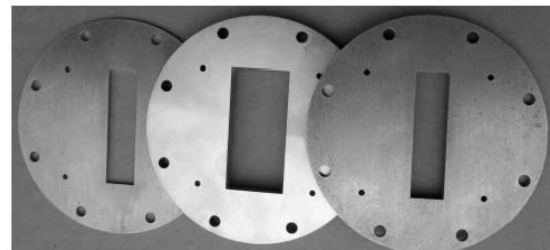


Figure 4. Brass aperture plates forming the fabricated waveguide verification standard.

4. COMPUTATION OF S -PARAMETERS OF WAVEGUIDE STANDARD USING MODE MATCHING

The mode matching approach is described in several References [25–27], and the specific details for the waveguide standard are given in [20]. Thus, only a brief outline is given here. Consider the geometry of the adopted waveguide standard shown in Fig. 1. Perfectly conducting apertures are positioned at $z = 0$ and $z = z_2$ with thickness Δ^ℓ and Δ^r , respectively. Although the adopted standard is longitudinally symmetric, the thicknesses of the apertures are allowed to be different so that the effects of manufacturing errors may be evaluated. The width of the apertures are the same as the width of the empty waveguide, a , while the vertical openings are describe by the height positions y_1^ℓ and y_2^ℓ for the left aperture, and y_1^r and y_2^r for the right aperture. The waveguide extensions are assumed to be of sufficient length such that, even though a full spectrum of higher order modes is produced at the apertures, only a TE_{10} mode is received at the measurement ports.

Assume a TE_{10} mode is incident from the transmitting extension $z < 0$. Interaction of this field with the aperture at $z = 0$ generates an infinite spectrum of modes in each of the waveguide sections. However, because of the symmetry of the incident field, only the $\text{TE}_{1,v}$ and $\text{TM}_{1,v}$ modes are excited with nonzero amplitude [28]. The transverse fields in each waveguide section may thus be written as a modal series, with terms representing both forward and reverse traveling waves. An identical number of modes, N , is used in each region. The modal amplitudes are determined by applying the boundary conditions on the transverse fields \vec{E}_t and \vec{H}_t at the interfaces between the full waveguide and the aperture regions. This produces a system of functional equations that may be transformed into a system of linear equations by applying appropriate testing operators. The result is a system of linear equations that may be written in terms of an $8N \times 8N$ partitioned matrix. Note that all of the integrals may be computed in closed form, and that many matrix entries are repeated or zero. This allows the matrix to be filled rapidly and leads to the overall efficiency of the mode-matching approach compared to more generic numerical electromagnetic techniques such as finite elements. Explicit expressions for the matrix entries are given in [20].

Once the modal coefficients are found by solving the matrix equation, the sample-plane S -parameters of the verification standard are given by

$$S_{11} = \frac{a_1^-}{a_1^+} \quad (4)$$

$$S_{21} = \frac{f_1^+}{a_1^+}. \quad (5)$$

where a_1^+ is the amplitude of the incident TE_{10} mode in the transmitting section ($z < 0$), a_1^- is the amplitude of the reflected TE_{10} mode in the transmitting section, and f_1^+ is the amplitude of the forward-traveling TE_{10} mode in the receiving section ($z > z_3$).

It is interesting to note that the S -parameters of two-port networks consisting of waveguide irises can be mathematically modeled with good accuracy using a rational multinomial. This allows for rapid evaluation during network optimization by using Cauchy interpolation. Although this approach was not implemented, it is potentially useful for rapid optimization of waveguide standard designs. The interested reader is directed to [21].

5. EXPERIMENTAL RESULTS

A sample waveguide verification standard was fabricated and measured at Michigan State University using materials on hand. The individual pieces, shown in Fig. 4, were constructed from brass using wire electrical discharge machining. The thicknesses of both the spacer and the apertures are slightly different than those specified for Table 1 due to available stock. The vertical positions of the aperture openings were influenced by the precision of the machining process.

5.1. Theoretical Material Parameters for the Fabricated Standard

The thicknesses and aperture positions of the constructed inserts were measured using precision calipers with a manufacturer-specified precision of ± 0.02 mm. Measurements were made at 15 positions on the inserts and the mean and standard deviation computed. The mean is taken as an estimation of the expected dimension, while the standard deviation is taken to be the uncertainty over the estimation. The results are shown in Table 1, along with the specified values for the optimized standard. Note that since the fabricated standard is not perfectly symmetric along z it is anticipated that measured values of μ and ϵ will have small imaginary parts.

Although the dimensions of the fabricated standard differ somewhat from those of the optimized standard used to establish Table 2, the fabricated standard is still useful, since the resulting values of μ and ϵ extracted from measurements of the fabricated standard are only slightly different than those for the optimized standard. (See Figs. 8 and 9 for the measured results.) Also, due to the availability of the mode-matching method, the dimensions of the fabricated standard may be used to establish the expected values of μ and ϵ , and these parameters used for verification of the measurement system. The mode matching method was used to compute the theoretical S -parameters for the fabricated geometry with the mean dimensions shown in Table 1. These S -parameters were then used to compute the values of μ and ϵ associated with the fabricated standard. Fig. 5 compares the real parts of these parameters with those found using the optimized design, while the imaginary parts are compared in Fig. 6. (Recall that the optimized design is longitudinally symmetric and thus produces zero imaginary parts.) While the difference in geometry does produce a shift in the material parameters, this shift is not excessive and the values still retain their desired properties of being near 6 while varying slowly across the measurement band.

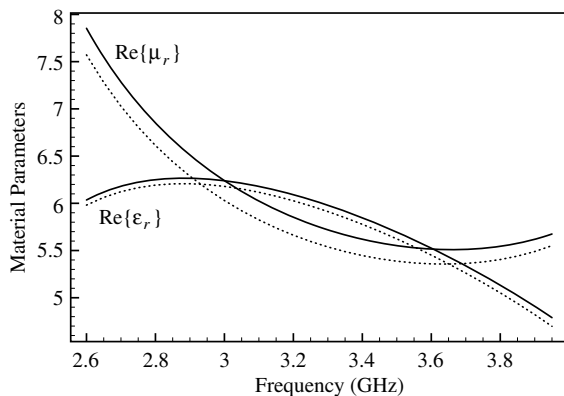


Figure 5. Real parts of relative permittivity and permeability for optimized geometry (solid line) and fabricated geometry (dotted line).

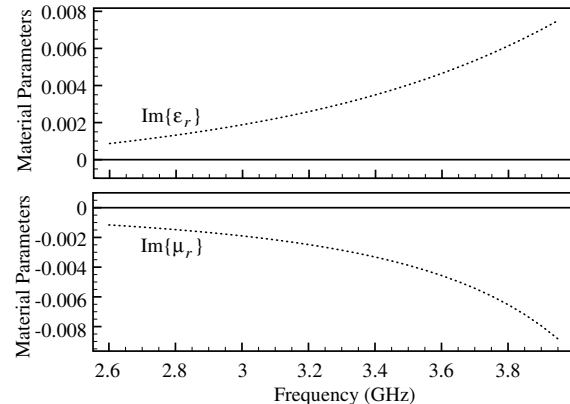


Figure 6. Imaginary parts of relative permittivity and permeability for optimized geometry (solid line) and fabricated geometry (dotted line).

5.2. Measured Material Parameters for the Fabricated Standard

Measurements of the S -parameters of the verification standard were made using an Agilent E5071C VNA. The verification standard was sandwiched between two 6 inch (152.4 mm) long sections of WR-284 commercial S-band waveguide, to act as extensions, with coaxial transitions attached at the ends. The VNA was calibrated at the ends of the waveguide extensions using the Through-Reflect-Line (TRL) method. Alignment pins were used for the different assemblies to ensure high repeatability of the measurements. Fig. 7 shows a diagram of the experimental setup, indicating the positions of the calibration planes. The positions of the S -parameter measurement planes are identical to those of the calibration planes. All measurements were made with VNA settings of -5 dBm source power, a measurement averaging factor of 64, and an IF bandwidth of 70 kHz. Finally, the material parameters were extracted using the measured values of S_{11} and S_{21} , assuming the average values of the insert dimensions shown in Table 1.

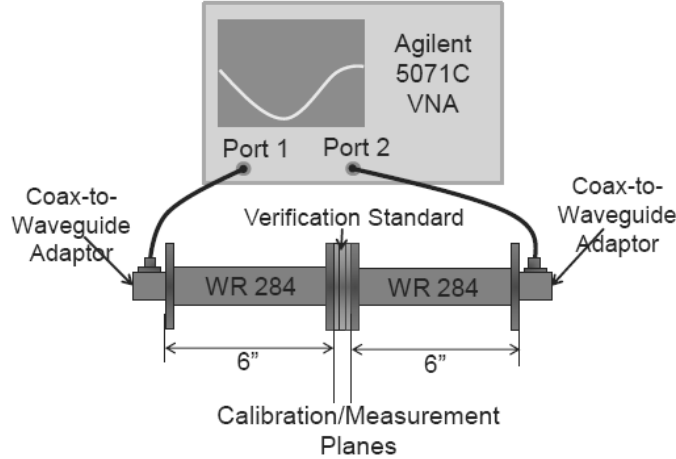


Figure 7. Experimental setup used to measure the S -parameters of the fabricated waveguide standard.

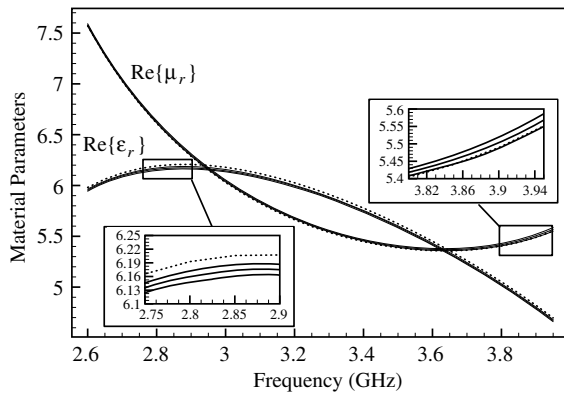


Figure 8. Real parts of relative permittivity and permeability extracted from 10 sets of measurements. Center solid line is the average of the measurements. Upper and lower lines show the 95% confidence intervals. Dotted line shows the material parameters extracted from the mode-matching S -parameters generated using the measured geometry.

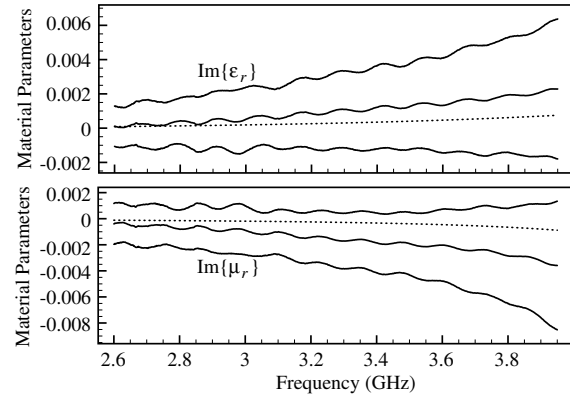


Figure 9. Imaginary parts of relative permittivity and permeability extracted from 10 sets of measurements. Center solid line is the average of the measurements. Upper and lower lines show the 95% confidence intervals. Dotted line shows the material parameters extracted from the mode-matching S -parameters generated using the measured geometry.

The measurement repeatability error was assessed by measuring the verification standard 10 separate times, with the VNA calibrated at the start of each set of measurements. Thus, the uncertainties of the setup including the VNA uncertainty are taken into account. The real parts of the material parameters extracted from the 10 measurements are shown in Fig. 8, while the imaginary parts are shown in Fig. 9. The center solid line in these figures represents the mean of the extracted values while the upper and lower solid lines define the 95% confidence intervals (\pm two standard deviations). The dotted lines show the theoretical material parameters from Figs. 5 and 6, found using the measured dimensions of the waveguide standard. Although the theoretical values for the imaginary parts lie within the 95% confidence intervals, the real parts lie just slightly outside these intervals, at least at some frequencies. This is shown more clearly in the insets, which zoom in on a chosen narrow region of the measurement band. There are several possible reasons for this, including calibration error, misalignment of the waveguide sections, imperfect electrical connections, variability in the thickness of the inserts, errors in the machining of the apertures, etc.. One error that can be modeled is produced by the uncertainty in the measured values of several of the geometric parameters. These include the

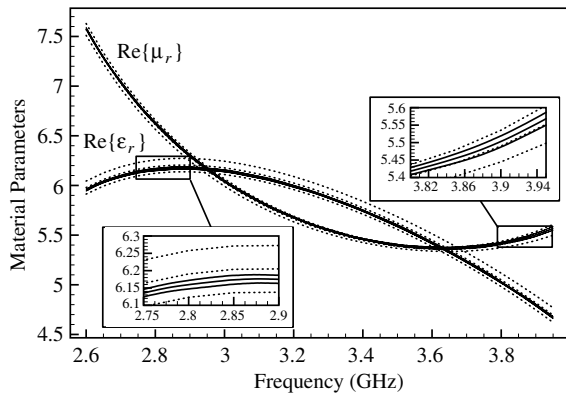


Figure 10. Real parts of the relative permittivity and permeability extracted from 10 sets of measurements (solid lines). Center solid line is the average of the measurements. Upper and lower solid lines show the 95% confidence intervals. Dotted lines show mode-matching results for 500 random trials. Center dotted line is the average and upper and lower dotted lines show the 95% confidence intervals.

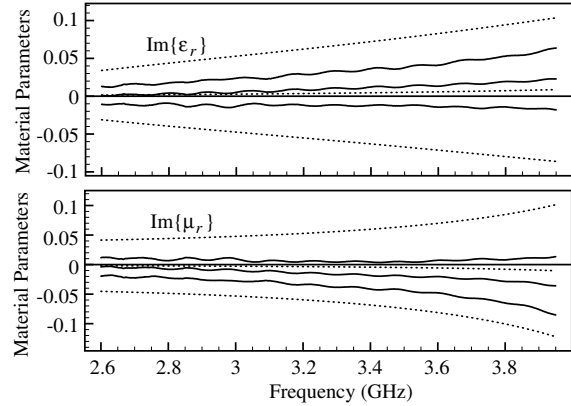


Figure 11. Imaginary parts of the relative permittivity and permeability extracted from 10 sets of measurements (solid lines). Center solid line is the average of the measurements. Upper and lower solid lines show the 95% confidence intervals. Dotted lines show mode-matching results for 500 random trials. Center dotted line is the average and upper and lower dotted lines show the 95% confidence intervals.

thicknesses of the aperture plates and spacer, and the sizes and vertical positions of the aperture openings. Unfortunately, the mode-matching approach does not allow the modeling of possible rotation of the apertures or spatial variations in thickness or opening size.

A Monte Carlo analysis was undertaken to determine the effects of geometry uncertainty on the extracted material parameters. Dimensions were generated randomly using a Gaussian distribution with a mean value set equal to the average of the measured values shown in Table 1, and a standard deviation equal to the standard deviation of the measured values shown in the table. The material parameters were extracted and the process repeated 500 times. The average values and the standard deviations of the extracted material parameters were calculated and are shown in Figs. 10 and 11. In these figures the measured data and their 95% confidence interval (solid triplet of lines) is shown along with the average Monte Carlo data and their 95% confidence interval (dashed triplet of lines). (Note that a more detailed analysis, with the sensitivity to each dimensional parameter examined separately, is considered in [20].) Clearly the measured data (including the 95% confidence interval) lie within the uncertainty interval of the Monte Carlo data for both real and imaginary parts of μ and ϵ , and the usefulness of the waveguide standard design procedure is demonstrated.

6. CONCLUSION

A waveguide standard is introduced to provide a surrogate material useful for verifying material characterization systems in the microwave spectrum. A surrogate is needed since no convenient materials are available that have slowly-varying, predictable and accurately reproducible magnetic characteristics at microwave frequencies. The standard is constructed from all metal parts, allowing for easy fabrication, and is straightforward to design using a mode-matching method for analysis. Specific dimensions are provided for an S-band standard to give relative permittivity and permeability near six when using the Nicolson-Ross-Weir method. The example standard is optimized using a genetic algorithm such that the extracted material properties are not highly sensitive to changes in the geometrical parameters, and so by reduce the need for tight manufacturing tolerances.

An example standard is measured, and the errors introduced by uncertainty in the dimensions of the machined parts are characterized. By showing that the measurement precision defined by the repeatability of the experiments is consistent with the error due to propagation of geometrical

uncertainties, the usefulness of the standard for verifying the proper operation of a waveguide material measurement system is demonstrated. Surrogate materials of similar geometries should be useful for verifying the performance of other types of material measurements systems that employ the Nicolson-Ross-Weir method, such as coaxial and stripline applicators. Design of these standards is left for future study.

ACKNOWLEDGMENT

The research reported in this paper was supported by the US Air Force Office of Scientific Research under grant FA9550-09-1-0182.

APPENDIX A.

Consider an isotropic, lossless, symmetric 2-port network with S -parameters S_{11} , S_{12} , S_{21} and S_{22} . The goal of this appendix is to establish the conditions under which values of μ and ϵ extracted from the S -parameters using the NRW equations will be real. The reader is referred to [20] for additional details.

The S -parameters of a lossless 2-port network satisfy the unitary condition $[S]^T[S^*] = [U]$. Writing out the matrix product gives the four equations

$$|S_{11}|^2 + |S_{21}|^2 = 1, \quad (\text{A1})$$

$$S_{11}S_{12}^* + S_{21}S_{22}^* = 0, \quad (\text{A2})$$

$$S_{12}S_{11}^* + S_{22}S_{21}^* = 0, \quad (\text{A3})$$

$$|S_{12}|^2 + |S_{22}|^2 = 1. \quad (\text{A4})$$

If the network is reciprocal, $S_{12} = S_{21}$ and (A2) and (A3) both become

$$S_{11}S_{21}^* + S_{21}S_{22}^* = 0. \quad (\text{A5})$$

If the network is also symmetric, such that $S_{11} = S_{22}$, then the allowed values of the S -parameters are subject to the two restrictions

$$|S_{11}|^2 + |S_{21}|^2 = 1, \quad (\text{A6})$$

$$S_{21r}S_{11r} + S_{21i}S_{11i} = 0. \quad (\text{A7})$$

Here S_{11r} and S_{11i} are the real and imaginary parts of S_{11} , respectively, and similarly for S_{21} .

The conditions (A6) and (A7) reveal the following relationship between S_{11} and S_{21} :

$$S_{21} = \pm jQ S_{11}, \quad Q = \sqrt{\frac{1 - |S_{11}|^2}{|S_{11}|^2}}. \quad (\text{A8})$$

Substituting into $V_1 = S_{21} + S_{11}$ and $V_2 = S_{21} - S_{11}$ gives

$$V_1 = S_{11}(1 \pm jQ), \quad V_2 = S_{11}(-1 \pm jQ), \quad (\text{A9})$$

which satisfy $|V_1| = |V_2| = 1$. Write

$$\Gamma = A \pm \sqrt{A^2 - 1}, \quad A = \frac{1 - V_1 V_2}{V_1 - V_2}. \quad (\text{A10})$$

Substituting for V_1 and V_2 yields $A = S_{11r}/|S_{11}|^2$ regardless of the sign chosen in (13); thus, A is real. Evaluating Γ then leads to two possible cases:

Case 1: $A^2 > 1$.

In this case Γ is real. Substituting Γ and V_1 into (2) then shows, with some effort, that $|P| = 1$. Using this in $\gamma = (\ln P - j2n\pi)/(-d)$ it is seen immediately that γ is imaginary. Finally, from (3) it is found that both μ and ϵ are real.

Case 2: $A^2 \leq 1$.

In this case $\Gamma = A \pm jB$, where $B = \sqrt{1 - A^2}$. This yields $|\Gamma| = 1$, which would represent total reflection in an actual material measurement scenario. Thus, this condition should be avoided when designing a material surrogate. Regardless, substituting for Γ it is found that

$$\frac{1 + \Gamma}{1 - \Gamma} = \pm j \sqrt{\frac{1 + A}{1 - A}} \quad (\text{A11})$$

and is thus imaginary. With some effort it can also be shown that

$$P = \frac{\text{Re}\{V_1 - \Gamma\}}{\text{Re}\{1 - \Gamma V_1\}} \quad (\text{A12})$$

and is thus real. So, if P is positive and $n = 0$ is chosen in $\gamma = (\ln P - j2n\pi)/(-d)$, γ will be real and again μ and ϵ will be real. However, if P is negative, γ will in general be complex and μ and ϵ will in general be complex.

REFERENCES

1. Dimiev, A., W. Lu, K. Zeller, B. Crowgey, L. C. Kempel, and J. M. Tour, "Low-loss, high-permittivity composites made from graphene nanoribbons," *Applied Materials & Interfaces*, Vol. 3, No. 12, 4657–4661, 2011.
2. Shirakata, Y., N. Hidaka, M. Ishitsuka, A. Teramoto, and T. Ohmi, "High permeability and low loss Ni-Fe composite material for high-frequency applications," *IEEE Trans. Magn.*, Vol. 44, No. 9, 2100–2106, 2008.
3. Verma, A., A. K. Saxena, and D. C. Dube, "Microwave permittivity and permeability of ferrite-polymer thick films," *Journal of Magn. Magn. Mater.*, Vol. 263, 228–234, 2003.
4. Smith, F. C., "Effective permittivity of dielectric honeycombs," *IEE Proc. Micro. Antennas Propag.*, Vol. 146, No. 1, 55–59, 1999.
5. Kempel, L., B. Crowgey, and J. Xiao, "Radiation by conformal patch antennas on a magneto-dielectric, low-density material," *3rd Euro. Conf. on Antennas Propag., EuCAP*, 2974–2976, 2009.
6. Damaskos, N. J., R. B. Mack, A. L. Maffett, W. Parmon, and P. L. Uslenghi, "The inverse problem for biaxial materials," *IEEE Trans. Microwave Theory Tech.*, Vol. 32, No. 4, 400–405, 1984.
7. Rothwell, E. J., A. K. Temme, and B. R. Crowgey, "Pulse reflection from a dielectric discontinuity in a rectangular waveguide," *Progress In Electromagnetics Research*, Vol. 97, 11–25, 2009.
8. Dudeck, K. E. and L. J. Buckley, "Dielectric material measurement of thin samples at millimeter wavelengths," *IEEE Trans. Instrum. Meas.*, Vol. 4, No. 5, 723–725, 1992.
9. Queffelec, P., M. Le Floch, and P. Gelin, "Non-reciprocal cell for the broad-band measurement of tensorial permeability of magnetized ferrites: Direct problem," *IEEE Trans. Microwave Theory Tech.*, Vol. 47, No. 4, 1999.
10. Lozano-Guerrero, A. J., F. J. Clemente-Fernandez, J. Monzo-Cabrera, J. L. Pedreno-Molina, and A. Diaz-Morcillo, "Precise evaluation of coaxial to waveguide transitions by means of inverse techniques," *IEEE Trans. Microwave Theory Tech.*, Vol. 58, No. 1, 229–235, 2010.
11. Williams, D. F., J. C. M. Wang, and U. Arz, "An optimal vector-network-analyzer calibration method," *IEEE Trans. Microwave Theory Tech.*, Vol. 51, No. 12, 2391–2401, 2003.
12. StatistiCAL, *National Institute of Standards and Technology (NIST)*, Boulder, CO, available online at <http://www.nist.gov/pml/electromagnetics/related-software.cfm>, last accessed Oct. 15, 2014.
13. Nicolson, A. M. and G. F. Ross, "Measurement of the intrinsic properties of materials by time-domain techniques," *IEEE Trans. Instrum. Meas.*, Vol. 19, No. 4, 377–382, 1970.
14. Weir, W. B., "Automatic measurement of complex dielectric constant and permeability at microwave frequencies," *Proc. IEEE*, Vol. 62, No. 1, 33–36, 1974.
15. Bogle, A., M. Havrilla, D. Nyquis, L. Kempel, and E. Rothwell, "Electromagnetic material characterization using a partially-filled rectangular waveguide," *Journal of Electromagnetic Waves and Applications*, Vol. 19, No. 10, 1291–1306, 2005.

16. Lambert, K. M. and C. L. Kory, "Notch filter insert for rectangular waveguide as a reference standard for material characterization," *NASA Tech Briefs: LEW-18137-1*, Glenn Research Center, Cleveland, OH, 2006.
17. Fenner, R. A., E. J. Rothwell, and L. L. Frasch, "A comprehensive analysis of free-space and guided-wave techniques for extracting the permeability and permittivity of materials using reflection-only measurements," *Radio Sci.*, Vol. 47, No. 1, 1004–1016, 2012.
18. Havrilla, M. J. and D. P. Nyquist, "Electromagnetic characterization of layered materials via direct and de-embed methods," *IEEE Trans. Instrum. Meas.*, Vol. 55, No. 1, 158–163, 2006.
19. Ihamouten, A., K. Chahine, V. Baltazart, G. Villain, and X. Derobert, "On variants of the frequency power law for the electromagnetic characterization of hydraulic concrete," *IEEE Trans. Instrum. Meas.*, Vol. 60, No. 11, 3658–3668, 2011.
20. Crowgey, B. R., "Rectangular waveguide material characterization: anisotropic property extraction and measurement validation," Ph.D. Dissertation, Michigan State University, East Lansing, MI, 2013.
21. Lamecki, P. K., P. K. Kozakowski, and M. Mrozowski, "Multimode, multiparametric surrogate models for fast design of waveguide components," *33rd European Microwave Conference*, 1369–1372, Munich, Germany, 2003.
22. Rothwell, E. J. and M. J. Cloud, *Electromagnetics*, 2nd Edition, CRC Press, Boca Raton, FL, 2008.
23. Castro, J., C. Morales, T. Weller, J. Wang, and H. Srikanth, "Synthesis and characterization of low-loss Fe₃O₄-PDMS magneto-dielectric polymer nanocomposites for RF applications," *IEEE 15th Annual Wireless and Microwave Technology Conference (WAMICON)*, 1–5, Tampa, FL, Jun. 6, 2014.
24. Ouedraogo, R., "Topology optimization of metamaterials and applications to RF component design," Ph.D. Dissertation, Michigan State University, East Lansing, MI, 2011.
25. Crowgey, B. R., O. Tuncer, J. Tang, E. J. Rothwell, B. Shanker, L. C. Kempel, and M. J. Havrilla, "Characterization of biaxial anisotropic material using a reduced aperture waveguide," *IEEE Trans. Instrum. Meas.*, Vol. 62, No. 10, 2739–2750, 2013.
26. Dester, G. D., E. J. Rothwell, and M. J. Havrilla, "Two-iris method for the electromagnetic characterization of conductor-backed absorbing materials using an open-ended waveguide probe," *IEEE Trans. Instrum. Meas.*, Vol. 61, No. 4, 1037–1044, 2012.
27. Dorey, S. P., M. J. Havrilla, L. L. Frasch, C. Choi, and E. J. Rothwell, "Stepped-waveguide material-characterization technique," *IEEE Antennas Propag. Mag.*, Vol. 46, No. 1, 170–175, 2004.
28. Harrington, R. F., *Time-harmonic Electromagnetic Fields*, John Wiley & Sons, Inc., New York, 2001.